Numerical study of all-optical slow-light delays via stimulated Brillouin scattering in an optical fiber

Zhaoming Zhu and Daniel J. Gauthier

Department of Physics, Duke University, Durham, North Carolina 27708

Yoshitomo Okawachi, Jay E. Sharping, and Alexander L. Gaeta

School of Applied and Engineering Physics, Cornell University, Ithaca, New York 14853

Robert W. Boyd

The Institute of Optics, University of Rochester, Rochester, New York 14627

Alan E. Willner

*Department of Electrical and Computer Engineering, University of Southern California,
Los Angeles, California 90089*

We study numerically all-optical slow-light delays in room-temperature single-mode optical fibers induced by stimulated Brillouin scattering. We consider the propagation of a pulse through a cw-pumped Brillouin fiber amplifier, where the carrier frequency of the pulse is tuned near the Stokes resonance. Pulse delay and broadening of the Stokes pulse are studied in the small-signal and gain-saturation regimes. Pulse delay is shown to be limited by saturation of the Brillouin amplifier. In the small-signal regime, both time delay and pulse broadening increase with increasing gain. In the gain-saturation regime, both time delay and broadening decrease with increasing gain, and the pulse even achieves advancement. Time delay of more than one pulse-width is observed with modest pulse distortion, and over one pulse-width advancement can be obtained with larger pulse distortion in the gain-saturation regime. © 2005 Optical Society of America

OCIS codes: 290.5900, 060.2430, 190.5890, 190.5530.

1. INTRODUCTION

There has been a great deal of recent interest in slow light, where the group velocity v_g of a pulse is much less than the speed of light in vacuum c. Slow light can be achieved, for example, using the large normal dispersion associated with a resonance of a material system.[1] Early slow-light research usually has used electromagnetically induced transparency[2–4] or coherent population oscillations,[5,6] in which a narrow transparency window is created within an absorbing resonance by an intense coupling laser field.

Slow light is also possible using the dispersion associated with a laser-induced amplifying resonance such as that arising from stimulated Raman scattering (SRS)[7,8] and stimulated Brillouin scattering (SBS). Recently Lee and Lawandy[7] demonstrated pulse delay in a $Ba(NO_3)_2$-crystal-based Raman amplifier, and more recently Okawachi *et al.*[9] and Song *et al.*[10] independently demonstrated slow light in an optical fiber SBS amplifier. One advantage of using an amplifying resonance due to stimulated scattering is that the resonance can be created at any wavelength through a simple change of the pump wavelength. The use of a single-mode optical fiber as the medium for SRS or SBS may offer additional advantages,

such as a low pump-power requirement owing to long interaction lengths and small mode areas, compatibility of the device with existing telecommunication systems, and room-temperature operation. Controllable slow light can be used in such applications as optical buffering, variable true time delay, and optical information processing. The slow-light technique based on SBS or SRS in optical fibers represents an important step toward implementing slow-light techniques for various applications.

In this paper, we analyze both analytically and numerically the slow-light effect due to SBS in single-mode optical fibers. The analysis shows that a large relative pulse delay of the Stokes pulse propagating through a SBS fiber amplifier can be achieved. Our results also show that pulse advancement (superluminal pulse propagation) can be achieved in the gain-saturation regime. This analysis complements and extends the recent experimental demonstrations of optically controllable pulse delays in optical fiber SBS amplifiers that were operated in the small-signal regime.[9,10]

This paper is organized as follows. Section 2 briefly describes the numerical model used in this study and explains the mechanism of slow light by SBS through small-signal linear analysis. In Section 3 we present the

numerical results, including pulse delay and pulse broadening of Stokes pulses in both small-signal and gain-saturation regimes. The implications of the results are discussed in Section 4, and conclusions are offered in Section 5.

2. NUMERICAL MODEL

We consider a Brillouin fiber amplifier where the pumping laser beam counterpropagates through the fiber with respect to the Stokes pulse. The SBS process can be described by one-dimensional coupled wave equations involving a backward pump wave (−*z* direction), a forward Stokes wave (+*z* direction), and a backward acoustic wave. Under the slowly varying envelope approximation (SVEA), the three-wave coupled wave equations are written as[11–13]

$$-\frac{\partial E_p}{\partial z} + \frac{n_{fg}}{c}\frac{\partial E_p}{\partial t} = -\frac{\alpha}{2}E_p + ig_2 E_s \rho, \tag{1a}$$

$$\frac{\partial E_s}{\partial z} + \frac{n_{fg}}{c}\frac{\partial E_s}{\partial t} = -\frac{\alpha}{2}E_s + ig_2 E_p \rho^*, \tag{1b}$$

$$\frac{\partial \rho}{\partial t} + \left(\frac{\Gamma_B}{2} - i\Delta\omega\right)\rho = i\frac{g_1}{\eta}E_p E_s^*. \tag{1c}$$

Here E_p, E_s, and ρ are the field amplitudes of the pump wave, the Stokes wave, and the acoustic wave, respectively; n_{fg} is the group index of the fiber mode; α is the loss coefficient of the fiber; $\Gamma_B/2\pi$ is the bandwidth (FWHM) of the Brillouin resonance, $\Delta\omega = (\omega_{p0} - \Omega_B) - \omega_{s0} = \omega_0 - \omega_{s0}$ is the detuning from the SBS gain line-center ω_0; Ω_B is the SBS frequency shift; $\omega_{p0}(\omega_{s0})$ is the center angular frequency of the pump (Stokes) wave; $g_1 = \gamma_e \epsilon_0 \Omega_B/(4v_a^2)$; $g_2 = \omega_{p0}\gamma_e/(4cn_f\rho_0)$; $\eta = \frac{1}{2}c\epsilon_0 n_f$; γ_e is the electrostriction coefficient of the fiber; ϵ_0 is the vacuum permittivity; v_a is the speed of the acoustic wave; n_f is the modal index of the fiber mode; and ρ_0 is the material density. In writing Eqs. (1a)–(1c), we have normalized E_p and E_s such that $|E_p|^2$ and $|E_s|^2$ are the optical intensity of the pump and Stokes waves, respectively.

For a sufficiently weak Stokes field, the cw pump is undepleted, and Eqs. (1a)–(1c) can be simplified as

$$\frac{\partial E_s}{\partial z} + \frac{n_{fg}}{c}\frac{\partial E_s}{\partial t} = ig_2 E_p \rho^*, \tag{2a}$$

$$\frac{\partial \rho^*}{\partial t} + \left(\frac{\Gamma_B}{2} + i\Delta\omega\right)\rho^* = -i\frac{g_1}{\eta}E_p^* E_s, \tag{2b}$$

where we have neglected the fiber loss (i.e., $\alpha = 0$). Transforming Eqs. (2a) and (2b) into the frequency domain,

one obtains

$$\frac{\partial \widetilde{E}_s}{\partial z} - i(\omega - \omega_{s0})\frac{n_{fg}}{c}\widetilde{E}_s = ig_2 E_p \widetilde{\rho}^*, \tag{3a}$$

$$\left[\frac{1}{2}\Gamma_B - i(\omega - \omega_{p0} + \Omega_B)\right]\widetilde{\rho}^* = -i\frac{g_1}{\eta}E_p^*\widetilde{E}_s, \tag{3b}$$

where $\widetilde{E}_s(\widetilde{\rho}^*)$ is the Fourier transform of $E_s(\rho^*)$. Substituting $\widetilde{\rho}^*$ from Eq. (3b) to Eq. (3a) yields

$$\frac{\partial \widetilde{E}_s}{\partial z} = i(\omega - \omega_{s0})\frac{n_{fg}}{c}\widetilde{E}_s + \frac{\frac{1}{2}g_0 I_p}{1 - i2\delta\omega/\Gamma_B}\widetilde{E}_s, \tag{4}$$

where $g_0 = 4g_1 g_2/(\eta\Gamma_B)$ is the line-center gain factor, $\delta\omega = \omega - \omega_{p0} + \Omega_B$, and I_p is the pump intensity.

By comparing Eq. (4) with the general SVEA wave equation in the frequency domain for a Stokes pulse propagating in +z direction, i.e., $\partial\widetilde{E}_s/\partial z = i[k_s(\omega) - k_s(\omega_{s0})]\widetilde{E}_s$, we find the equivalent wave vector for the Stokes wave

$$k_s(\omega) = n_f\frac{\omega}{c} - i\frac{\frac{1}{2}g_0 I_p}{1 - i2\delta\omega/\Gamma_B} \equiv \frac{\omega}{c}\widetilde{n}_s. \tag{5}$$

From Eq. (5), it is seen that the effective complex index for the Stokes wave is given by

$$\widetilde{n}_s = n_f - i\frac{c}{2\omega}\frac{g_0 I_p}{1 - i2\delta\omega/\Gamma_B}. \tag{6}$$

From Eq. (6), it is seen that the Stokes wave experiences gain and dispersion in the form of a Lorentzian-shaped resonance that is induced by the pump beam via the SBS process. The gain coefficient $g_s = -2(\omega/c)\mathrm{Im}(\widetilde{n}_s)$, refractive index $n_s = \mathrm{Re}(\widetilde{n}_s)$, and group index $n_g = n_s + \omega(\mathrm{d}n_s/\mathrm{d}\omega)$ are given by

$$g_s(\omega) = \frac{g_0 I_p}{1 + 4\delta\omega^2/\Gamma_B^2}, \tag{7a}$$

$$n_s(\omega) = n_f + \frac{cg_0 I_p}{\omega}\frac{\delta\omega/\Gamma_B}{1 + 4\delta\omega^2/\Gamma_B^2}, \tag{7b}$$

$$n_g(\omega) = n_{fg} + \frac{cg_0 I_p}{\Gamma_B}\frac{1 - 4\delta\omega^2/\Gamma_B^2}{(1 + 4\delta\omega^2/\Gamma_B^2)^2}, \tag{7c}$$

respectively. As shown in Fig. 1, large normal dispersion ($\mathrm{d}n_s/\mathrm{d}\omega > 0$) is associated with the gain resonance, which gives rise to an increase in the group index and therefore a decrease in group velocity $v_g = c/n_g$. The reduced group velocity of the Stokes pulse leads to a slow-light time delay in propagating through the fiber compared with the case in which the SBS process is absent. If we use the values for the common single-mode fiber SMF-28 at 1550 nm, mode area $A_{\mathrm{eff}} = 50\ \mu\mathrm{m}^2$, $\Gamma_B/2\pi = 40$ MHz, and $g_0 = 5 \times 10^{-11}$ m/W, Eqs. (7a)–(7c) give on-resonance $g_s = 0.1$ m^{-1}, and group-index change $n_g - n_{fg} \simeq 1.2 \times 10^{-3}$ for a cw pump power of 1 mW. We note that the SBS-induced group index change depends on the fiber type and the
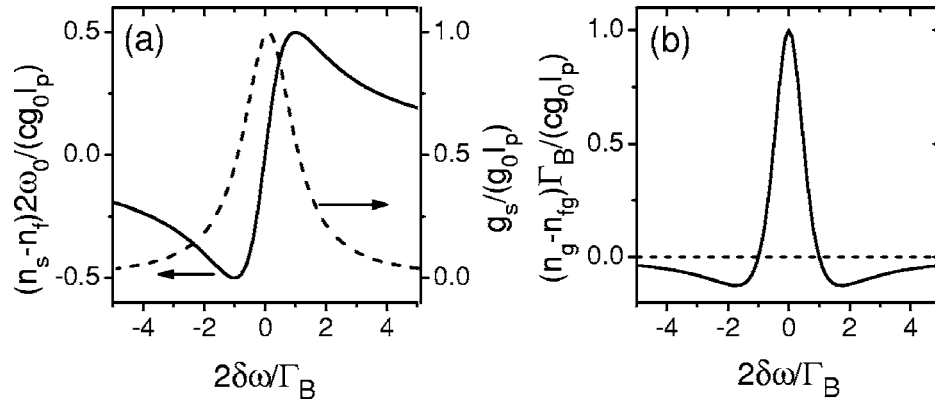
Fig. 1.   Large dispersion of the SBS resonance. (a) Gain (dashed curve) and refractive index (solid curve) of the resonance. (b) Group index of the resonance.

pump power. For the SMF-28e fiber used by Okawachi *et al.*,[9] the group-index change is about 3.4×10^{-4} at 1 mW pump power owing to the wider SBS bandwidth of the SMF-28e fiber ($\sim$70 MHz). For the standard single-mode fiber used by Song *et al.*,[10] the group-index change is estimated to be 1.3×10^{-3} at 1 mW pump power.

Using Eq. (6) and following the approach described by Boyd *et al.*,[14] we obtain the pulse delay ΔT_d of a Stokes pulse (defined as the difference between the transit times of the pulse with and without SBS):

$$\Delta T_d \equiv \frac{L}{c}(n_g - n_{fg})$$

$$= \frac{G}{\Gamma_B}\frac{1 - 4\delta\omega^2/\Gamma_B^2}{(1 + 4\delta\omega^2/\Gamma_B^2)^2}$$

$$\simeq \frac{G}{\Gamma_B}(1 - 12\delta\omega^2/\Gamma_B^2) \qquad \text{when } 4\delta\omega^2/\Gamma_B^2 \ll 1, \quad (8)$$

where $G = g_0 I_p L$ is the gain parameter whose exponential gives the small-signal gain, and L is the fiber length. The maximum delay occurs at the peak of the Brillouin gain ($\delta\omega = 0$) and is simply given by

$$\Delta T_d = G/\Gamma_B. \qquad (9)$$

The proportionality of ΔT_d to G shows that the delay is controllable by adjusting G, which is proportional to pump intensity I_p. Equation (9) gives $\Delta T_d \simeq 0.92$ ns/dB for $\Gamma_B/2\pi = 40$ MHz. Okawachi *et al.*[9] measured $\Delta T_d \sim 0.52$ ns/dB for a SMF-28e fiber, and Song *et al.*[10] obtained $\Delta T_d \sim 1$ ns/dB for a standard single-mode fiber.

On-resonance and for a long Gaussian-shaped Stokes pulse of duration τ_{in} (FWHM), the pulse emerging from the optical fiber is also Gaussian shaped with a longer pulse length τ_{out} (FWHM), where the pulse-broadening factor B is given by

$$B \equiv \frac{\tau_{\text{out}}}{\tau_{\text{in}}} = \left(1 + \frac{16 \ln 2}{\tau_{\text{in}}^2 \Gamma_B^2}G\right)^{1/2}. \qquad (10)$$

Using the relation between pulse broadening and delay, we find that the relative time delay for a fixed value of B is given by

$$\frac{\Delta T_d}{\tau_{\text{in}}} = \left(\frac{B^2 - 1}{16 \ln 2}G\right)^{1/2}. \qquad (11)$$

Equation (10) shows that the pulse delay is always accompanied by pulse broadening. For example, $\Delta T_d/\tau_{\text{in}} \simeq 1.6$ when $G = 10$ and $B = 2$. For a short-duration input pulse, both ΔT_d and B deviate from the values predicted by Eqs. (8) and (10), and the output pulse is distorted owing to higher-order dispersion, as will be shown in the numerical simulations.

3. NUMERICAL RESULTS

The small-signal analysis described above provides useful insight into the mechanisms of the slow-light effect of SBS in optical fibers. However, it cannot be used in situations where a pulsed pump beam is used, where the pump beam is depleted, or for short Stokes pulses. In this section, we solve Eqs. (1a)–(1c) numerically using the method of characteristics[15] to determine how such effects modify slow light via SBS. In our numerical simulations, we assume that the pump is cw and that the Gaussian-shaped Stokes pulse is on the SBS line center ($\delta\omega = 0$) and has no frequency chirp, and we use the following parameters for a SMF-28 fiber: $L = 50$ m, $\lambda = 1550$ nm, $n_{fg} = 1.45$, $A_{\text{eff}} = 50$ μm^2, $\alpha = 0.2$ dB/km, $\Gamma_B/2\pi = 40$ MHz, and $g_0 = 5 \times 10^{-11}$ m/W.

We first consider the pulse delay ΔT_d and pulse broadening B as a function of the gain parameter G for different input pulse widths. Figure 2 shows the variations in ΔT_d and B as functions of G for a relatively long pulse of FWHM of 120 ns (its FWHM bandwidth of $\sim$3.7 MHz is much smaller that the SBS gain bandwidth of 40 MHz). The peak power of the input Stokes pulse is 0.1 μW. The gain parameter G is limited up to the Brillouin threshold of $\sim$25.[12] For $G \sim 25$, photons spontaneously scattered from thermal phonons near the entrance face of the fiber are amplified by a factor of $\sim$exp(25), resulting in the generation of a Stokes field at the output that saturates the pump field in the absence of any input Stokes field.[12] Therefore the spontaneous Brillouin scattering will limit the maximum useful gain parameter G to be below the Brillouin threshold of $\sim$25. As can be seen in Fig. 2(a), ΔT_d increases linearly with G and agrees well with the analytic prediction (dashed curve) by Eq. (9) when G is

small ($\lesssim 8$). This is expected, since the cw pump is essentially unaffected when the gain is small and thus the small-signal analysis is valid. At larger G, gain saturation (pump depletion) causes ΔT_d to deviate from the analytic result: ΔT_d increases slowly with G and reaches its maximum before decreasing with G. Simulations with other peak powers show that gain saturation starts at different G for Stokes pulses of different peak powers, and that a lower peak power pulse enters the gain-saturation regime at a higher gain. Gain saturation is thus seen to limit the maximum time delay that a Stokes pulse can experience for a given input power.

In the gain-saturation regime, the time delay ΔT_d decreases with increasing G and even becomes negative (i.e., the pulse experiences advancement instead of delay). This behavior of ΔT_d can be explained by gain-saturation-induced pulse advancement, because the amplified pulse is intense enough to deplete the pump, and the leading edge of the pulse experiences higher amplification than the trailing edge. The pulse advancement (superluminal pulse propagation) is a typical feature in a saturated amplifier and was first studied by Basov *et al.*[16] and has since attracted considerable interest (see Ref. 1 and references therein).

The calculated pulse-broadening factor also agrees well with the analytic result (dashed curve) given by Eq. (10) when G is small, as shown in Fig. 2(b). At larger G, the numerical result deviates from the analytic result because of gain saturation. In the gain-saturation regime, the pulse even narrows a little bit because of pulse distortion. Figure 2(c) shows the normalized output pulse shapes at $G=0$, 12, and 25, respectively. Evidently, the output pulse with a maximum time delay (~ 43 at $G=12$) has little distortion, whereas the output pulse is advanced by ~ 114 ns in the highly saturated regime ($G=25$) but is distorted substantially.

For the purpose of comparison, we show in Fig. 3 the scenario for a relatively short pulse of 20 ns (FWHM) and of the same peak power of 0.1 μW. Both ΔT_d and B deviate substantially from and are smaller than the analytic results (shown as dashed curves), even when G is small. The reason is that the wide spectral content of the short pulse (in comparison with the SBS gain bandwidth) makes third-order dispersion important in the pulse propagation, which is neglected in obtaining Eqs. (9) and (10). The smallness of the numerically calculated ΔT_d compared with the analytic one can also be simply explained as following: Part of the input spectrum experiences a delay given by Eq. (9), whereas an appreciable fraction of the spectral components experience smaller delays because of frequency detuning, as shown in Eq. (8), resulting in a pulse delay that is smaller than that is predicted by Eq. (9). Compared with the 120-ns pulse, the 20-ns pulse reaches the saturation regime at a larger G,
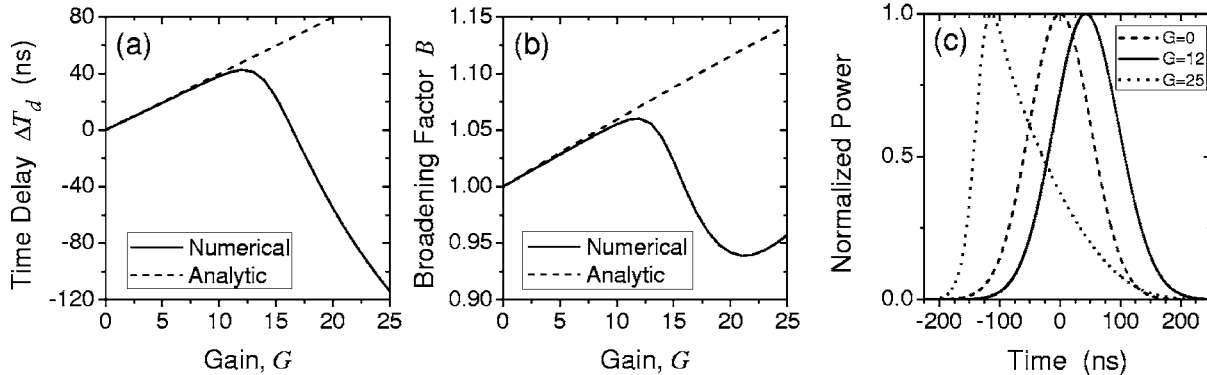

Fig. 2. (a) Pulse delay versus gain. (b) Pulse broadening factor versus gain. (c) Normalized output pulses at $G=0$, 12, and 25 (the output peak powers are 9.98×10^{-8} W, 1.30×10^{-2} W and 0.88 W, respectively). The input Stokes pulse has a peak power of 0.1 μW and a FWHM width of 120 ns. The dashed curves in (a) and (b) are obtained from Eqs. (9) and (10), respectively.
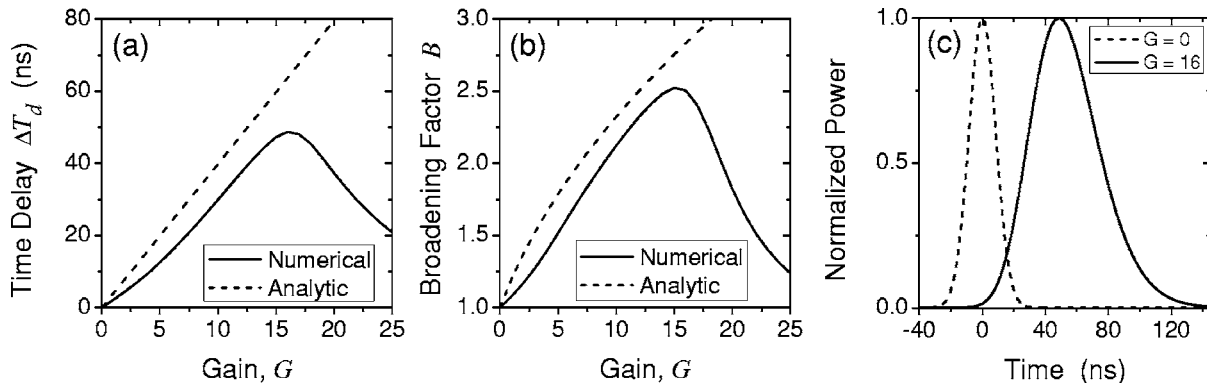

Fig. 3. (a) Time delay versus gain. (b) Broadening factor versus gain. (c) Normalized output pulse powers at $G=0$ and 16 (the output peak powers are 9.98×10^{-8} W and 9.99×10^{-2} W, respectively). The input Stokes pulse has a peak power of 0.1 μW and a FWHM width of 20 ns. The dashed curves in (a) and (b) are obtained from Eqs. (9) and (10), respectively.
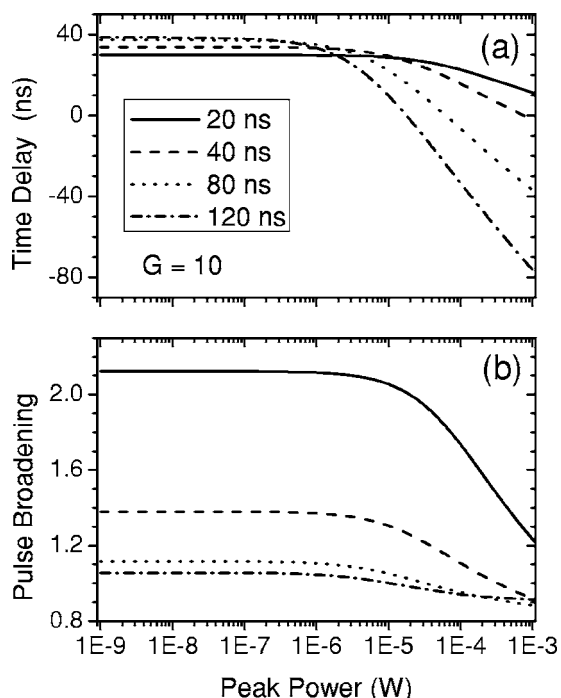
Fig. 4. (a) Pulse delay versus input peak power and (b) pulse-broadening factor versus input peak power for different input pulse widths. The gain parameter G is fixed at 10. The FWHM width of the input pulse is labeled in (a).

and the maximum time delay is accordingly larger. At the same time, however, pulse broadening is significant owing to the broader bandwidth of the pulse. In Fig. 3(c), we plot the normalized output Stokes pulses at $G=0$ and 16, illustrating the pulse distortion at a maximum delay of ~49 ns at $G=16$. The relative time delay achieves its maximum ~2.5 at $G=16$ in this case. The maximum relative time delay could be larger for lower-power or shorter Stokes pulses, but it is achieved at the cost of large temporal broadening and distortion.

Next, we look at the time delay and pulse broadening as a function of input peak power for different pulse widths at a fixed gain. As we see in Fig. 4, the time delay and pulse broadening are constant for low peak power and are reduced at high peak power because of gain saturation. Longer pulses obtain both larger time delay and less pulse broadening, and there is a upper limit for the maximum time delay, as given by Eq. (9).

We also investigate the time delay and pulse broadening as a function of the Stokes input pulse width for different input peak powers at a fixed gain. As shown in Fig. 5, at a fixed gain $G=10$, higher-power pulses start to deplete the pump at shorter pulsewidths and achieve a smaller maximum time delay, while lower peak-power pulses have the opposite trend and tend to obtain a maximum time delay independent of the input pulse width. Pulse broadening is seen to depend only on the input pulse width and is negligible for longer pulses.

Further simulations indicate that the maximum time delay for an input Stokes pulse is determined approximately by the pulse energy and is independent of the input pulse width when the input pulse width is much longer than the lifetime of the acoustic wave ($\tau_a=1/\Gamma_B$ is

~4 ns in this study). Figure 6 shows an example of the simulations. While the maximum time delay is nearly the same for the pulses with the same energy, the pulse delay changes with the input pulse width in a different manner in the gain-saturation regime: For longer (shorter) pulses the time delay decreases more quickly (slowly) with gain G. This indicates that the gain-saturation-induced advancements are larger for longer pulses.

Finally, we look at the variation of the relative time delay $\Delta T_d/\tau_{in}$ with the input Stokes pulse width τ_{in} at a fixed gain parameter G. For $G=10$, such a plot can be inferred from Fig. 5(a) with the time delay ΔT_d divided by the corresponding input pulse width τ_{in}. Figure 7 shows $\Delta T_d/\tau_{in}$ versus τ_{in} for $G=10$ in the small-signal limit, which is the upper bound of the curves for input pulses of different peak powers. The corresponding pulse-broadening factor B is also shown in Fig. 7 for better visualization. Apparently, the use of short Stokes pulses tends to achieve large relative delays, but at the expense of large pulse broadening. If we require the pulse-broadening factor be ≤2, then the maximum relative delay achievable for $G=10$ is about 1.4 at an input width of ~22 ns and with a peak power $\lesssim5$ μW.

4. DISCUSSION
Depending on the applications, one may want to delay a pulse by a certain amount of time ΔT_d or want a specific relative time delay $\Delta T_d/\tau_{in}$. For both cases, the analytical
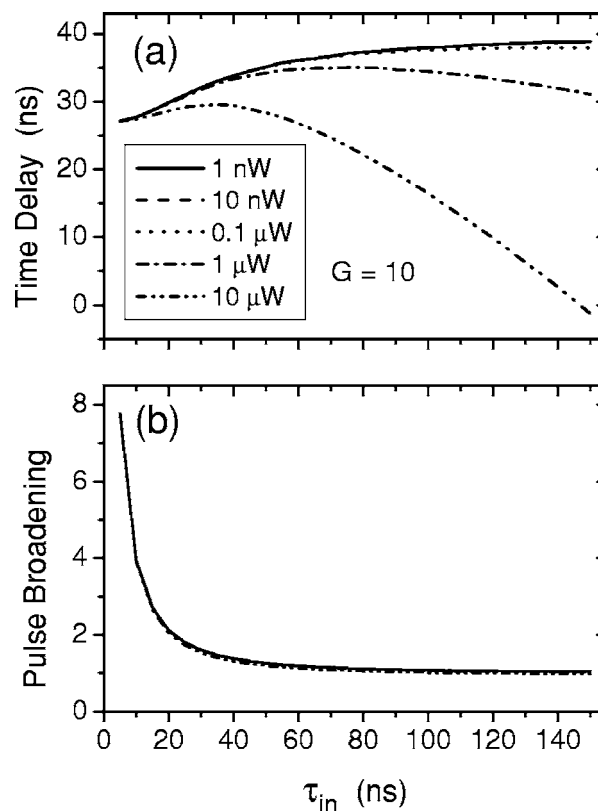

Fig. 5. (a) Pulse delay versus input pulse width and (b) pulse-broadening factor versus input pulse width for different input peak powers. The gain parameter G is fixed at 10. The peak power of the input pulse is labeled in (a).

and numerical results presented in the previous sections can be applied. At a given gain-parameter G, the maximum achievable time delay is that given by the small-signal limit value [Eq. (9)], i.e., G/Γ_B. In the small-signal regime, a long Stokes pulse experiences a larger time delay ΔT_d than a short Stokes pulse does with the same gain parameter, as shown in Figs. 2(a), 3(a), and 4(a). Gain saturation has been shown to limit the time delay to below the small-signal limit and even leads to pulse advancement. Furthermore, the maximum useful gain parameter is limited by spontaneous Brillouin scattering to below the Brillouin threshold of about 25. As shown in Fig. 7, the use of short pulses can obtain large relative pulse delays, but with large pulse broadening that may render the delay useless. Ultimately, the maximum achievable relative time delay is given by Eq. (11) for a designated pulse-broadening factor B. For $G=25$ and $B=2$, we find from Eq. (11) that $\Delta T_d/\tau_{in}=2.6$.

The limitation on the maximum achievable ΔT_d and $\Delta T_d/\tau_{in}$ can be circumvented, for example, by cascading multiple SBS fiber amplifiers separated by attenuators. The amplified Stokes pulses from the preceding amplifier are attenuated and delayed in the next amplifier. This cascading scheme allows one to increase the gain parameter G without the problem of gain saturation, as long as each SBS amplifier is operated in the small-signal regime. In this case, the analytic results given by Eqs. (9)–(11) are still applicable for long Stokes pulses, with G being the sum of the gain parameters of all the cascaded amplifiers.

As has been shown analytically and numerically, the time delay of the Stokes pulse is optically controllable by changing the pump intensity in the small-signal and
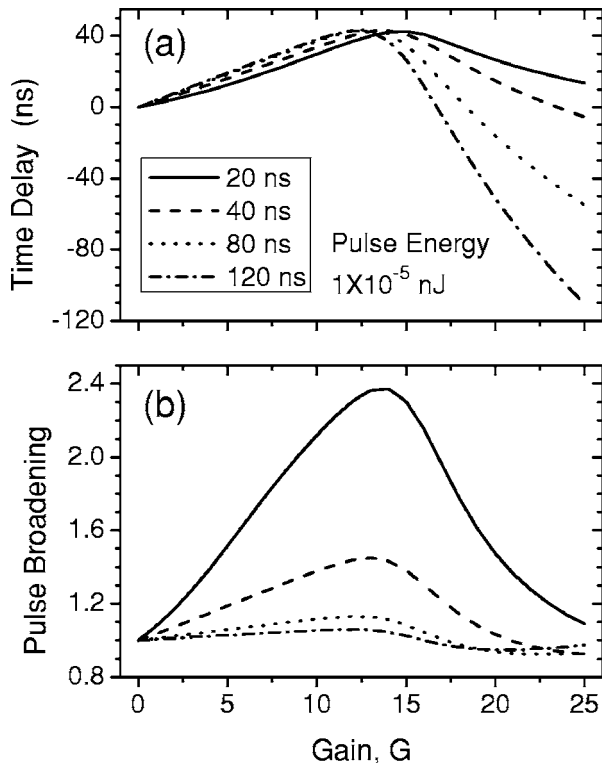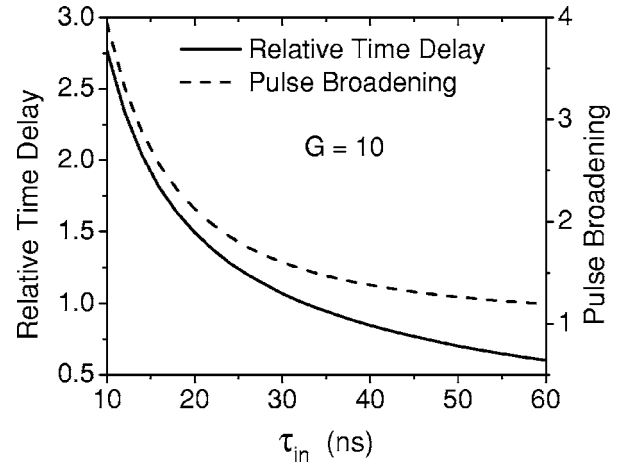

Fig. 7. Relative time delay and pulse broadening versus input pulse width at $G=10$. A maximum relative time delay of about 1.4 is obtained using ~ 22 ns pulses if the pulse broadening factor of $\leqslant 2$ is required.

gain-saturation regimes. In the small-signal regime, the time delay ΔT_d increases linearly with gain G, and the pulses do not interfere with each other if they are well separated. In the gain-saturation regime, the time delay ΔT_d decreases with gain G in a linear fashion, and pulse advancement can be achieved at cost of appreciable pulse distortion (a steep leading edge and a long trailing edge). The tunability of SBS-induced optical delays may find such applications as all-optical buffering in fiber-optic communication systems, and optical information processing.

By changing the SBS gain, the delays described in this paper can be tuned from small fractions of a pulsewidth to several pulsewidths. There are potential dynamic network scenarios for which we might want to use such a tunable all-optical delay element that keeps the data pulses in the optical domain. Buffering in an optical switch is one example,[17] but buffers of just 1–2 data-bit lengths tend to be of limited value. Three all-optical applications of small relative delays are (i) accurate synchronization of two different optical-data streams such that they can be efficiently switched or bit interleaved[18]; (ii) data bit equalization of degrading effects using a tapped delay line, for which a series of weighted delays would take a corrupted optical pulse and put the optical energy back into its appropriate bit time slot[19]; and (iii) true time delay for optical phased-array radar.[20,21]

Importantly, we must concern ourselves with the "quality" of the output data pulses, especially if the output of the delay element will be transmitted over some distance of dispersive optical fiber. It would be crucial to fully evaluate the time- and frequency-domain characteristics of the delayed pulses. From the analysis, we know that the pulses are broadened over time. If their frequency components are also affected by the delay element, then the pulse will behave differently when it passes through fiber. Chirp, extinction ratio, noise, polarization dependence, and bit error rates of the output optical pulses are all important parameters to measure.

5. CONCLUSION

In summary, we have studied theoretically the slow-light effect via SBS in optical fibers. In the small-signal regime,

Fig. 6. (a) Pulse delay versus gain and (b) pulse-broadening factor versus gain. The input pulse energy is fixed at 1×10^{-5} nJ. The FWHM width of the input pulse is labeled in (a).

the time delay increases linearly with gain. In the saturated regime, the time delay decreases with gain and pulse advancement can be obtained. Accompanying the time delay is pulse broadening and distortion, which, together with the gain saturation and spontaneous Brillouin scattering, limits the achievable maximum (relative) time delay. The results show a significant improvement in terms of relative delay and bandwidth over previous demonstrations of slow light in solids.[5,6] Additionally, these Brillouin slow-light results strongly suggest that analogous slow-light delays can be achieved using stimulated Raman scattering in optical fibers at telecommunication data rates (>10 Gbits/s).

ACKNOWLEDGMENTS

REFERENCES

1. R. W. Boyd and D. J. Gauthier, "'Slow' and 'fast' light," in *Progress in Optics*, E. Wolf, ed. (Elsevier, 2002), Vol. 43, Chap. 6, pp. 497–530.
2. L. V. Hau, S. E. Harris, Z. Dutton, and C. H. Behroozi, "Light speed reduction to 17 meters per second in an ultracold atomic gas," Nature **397**, 594–598 (1999).
3. M. M. Kash, V. A. Sautenkov, A. S. Zibrov, L. Hollberg, G. R. Welch, M. D. Lukin, Y. Rostovtsev, E. S. Fry, and M. O. Scully, "Ultraslow group velocity and enhanced nonlinear optical effects in a coherently driven hot atomic gas," Phys. Rev. Lett. **82**, 5229–5232 (1999).
4. A. V. Turukhin, V. S. Sudarshanam, M. S. Shahriar, J. A. Musser, B. S. Ham, and P. R. Hemmer, "Observation of ultraslow and stored light pulses in a solid," Phys. Rev. Lett. **88**, 023602 (2002).
5. M. S. Bigelow, N. N. Lepeshkin, and R. W. Boyd, "Observation of ultraslow light propagation in a ruby crystal at room temperature," Phys. Rev. Lett. **90**, 113903 (2003).
6. M. S. Bigelow, N. N. Lepeshkin, and R. W. Boyd, "Superluminal and slow light propagation in a room-temperature solid," Science **301**, 200–202 (2003).
7. K. Lee and N. M. Lawandy, "Optically induced pulse delay in a solid-state Raman amplifier," Appl. Phys. Lett. **78**, 703–705 (2001).
8. F. L. Kien, J. Q. Liang, and K. Hakuta, "Slow light produced by far-off-resonance Raman scattering," IEEE J. Sel. Top. Quantum Electron. **9**, 93–101 (2003).
9. Y. Okawachi, M. S. Bigelow, J. E. Sharping, Z. Zhu, A. Schweinsberg, D. J. Gauthier, R. W. Boyd, and A. L. Gaeta, "Tunable all-optical delays via Brillouin slow light in an optical fiber," Phys. Rev. Lett. **94**, 153902 (2005).
10. K. Y. Song, M. G. Herráez, and L. Thévenaz, "Observation of pulse delaying and advancement in optical fibers using stimulated Brillouin scattering," Opt. Express **13**, 82–88 (2005).
11. R. W. Boyd, *Nonlinear Optics* (Academic, 1992).
12. G. P. Agrawal, *Nonlinear Fiber Optics*, 3rd ed. (Academic, 2001).
13. M. J. Damzen, V. I. Vlad, V. Babin, and A. Mocofanescu, *Stimulated Brillouin Scattering* (IOP, 2003).
14. R. W. Boyd, D. J. Gauthier, A. L. Gaeta, and A. E. Willner, "Maximum time delay achievable on propagation through a slow-light medium," Phys. Rev. A **71**, 023801 (2005).
15. C. M. de Sterke, K. R. Jackson, and B. D. Robert, "Nonlinear coupled-mode equations on a finite interval: a numerical procedure," J. Opt. Soc. Am. B **8**, 403–412 (1991).
16. N. G. Basov, R. V. Ambartsumyan, V. S. Zuev, P. G. Kryukov, and V. S. Letokhov, "Propagation velocity of an intense light pulse in a medium with inverted population," Sov. Phys. Dokl. **10**, 1039–1040 (1966).
17. D. Hunter, M. Chia, and I. Andonovic, "Buffering in optical packet switches," J. Lightwave Technol. **16**, 2081–2095 (1998).
18. S. Hamilton and B. Robinson, "40-Gb/s all-optical packet synchronization and address comparison for OTDM networks," IEEE Photonics Technol. Lett. **14**, 209–211 (2002).
19. H. Bulow, F. Buchali, W. Baumert, R. Ballentin, and T. Wehren, "PMD mitigation at 10 Gbits/s using linear and nonlinear integrated electronic equaliser circuits," Electron. Lett. **36**, 163–164 (2000).
20. R. Minasian and K. Alameh, "Optical-fiber grating-based beamforming network for microwave phased arrays," IEEE Trans. Microwave Theory Tech. **45**, 1513–1519 (1997).
21. A. Rader and B. Anderson, "Demonstration of a linear optical true-time delay device by use of a microelectromechanical mirror array," Appl. Opt. **42**, 1409–1417 (2003).